2014 IEEE/RSJ International Conference on
Intelligent Robots and Systems (IROS 2014)
September 14-18, 2014, Chicago, IL, USA

Achieving Elastic Stability of Concentric Tube Robots Through Optimization of Tube Precurvature

Junhyoung Ha[1], *Member, IEEE*, Frank C. Park[2], *Fellow, IEEE*
and Pierre E. Dupont[3], *Fellow, IEEE*

***Abstract*— Minimally invasive surgery can involve navigating inside small cavities or reaching around sensitive tissues. Robotic instruments based on concentric tube technology are well suited to these tasks since they are slender and can be designed to take on shapes of high and varying curvature along their length. One limitation of these robots, however, is that elastic instabilities can arise when rotating one pre-curved tube inside another. While prior work has considered tubes of piecewise-constant pre-curvature, this paper proposes varying tube pre-curvature as a function of arc length as a means to enhance stability. Stability conditions for a planar tube pair are derived and used to define an optimal design problem. This framework enables solving for pre-curvature functions that achieve a desired tip orientation range while maximizing stability and respecting bending strain limits. Analytical and numerical examples of the approach are provided.**

I. INTRODUCTION

Concentric tube robots are a type of continuum robot that are comprised of nested combinations of pre-curved superelastic tubes [1]–[3]. The shape of these robots is determined by the bending and torsional elastic interaction of the tubes. Since they can be designed to take on complex 3D curves and possess sufficient stiffness to both steer through tissue and manipulate tools in body cavities, they are well suited to minimally invasive surgery [4]–[7].

One limitation, however, is that instabilities can arise in which torsional elastic energy is suddenly released through rapid untwisting of one or more tubes [1], [2]. Several approaches have been taken to address this issue. For example, robots designs can be constrained to be globally stable, i.e., not exhibit an instability anywhere in their workspace. Alternately, path planning can be used to avoid passing through unstable configurations [8].

Nevertheless, elastic instability imposes significant constraints on robot and workspace design. An important example, shown in Figure 1, is comprised of a pair of tubes of equal stiffness and with pre-curvatures that are independent of arc length. By rotating these tubes at their base, the combined curvature varies from the maximum pre-curvature value to zero. The latter configuration corresponds to a base rotation angle of π and is stable, for constant tube pre-curvatures, if and only if the following condition first derived in [9], [1] is met.

$$L\sqrt{(1+\nu)||\hat{u}_1||||\hat{u}_2||} = \sqrt{\beta_1\beta_2(1+\nu)} < \pi/2 \qquad (1)$$

[1]J. Ha and [2]F.C. Park are with the School of Mechanical Engineering, Seoul National University, Seoul, Korea. [3]P. E. Dupont is with the Department of Cardiovascular Surgery, Boston Children's Hospital, Harvard Medical School, Boston, Massachusetts, USA.

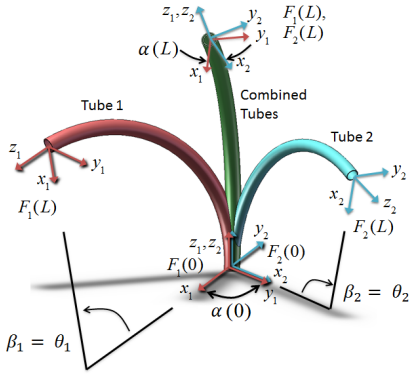

Fig. 1. Effect of torsional twisting when two curved tubes are combined. Tube coordinate frames are denoted by $F_i(s)$. The relative z-axis twist angle between frames $\alpha(s)$ varies from a maximum $\alpha(0)$ at the base to a minimum $\alpha(L)$ at the tip. The central angles $\beta_i = \theta_{tip,i}$ are proportional to the pre-curvature and to the tube length L.

In this equation, L is the tube length, ν is the Poisson's ratio of the tubes, and $\hat{u}_i$ and β_i are the pre-curvature and central angle of the i-th tube, respectively. When this condition is not met, base rotations produce a snapping rotational motion as the tube pair is straightened.

Viewed from different design perspectives, this stability condition places bounds on either the tube length L, the pre-curvatures, $\hat{u}_i$, or the central angles, β_i. In particular, two tubes of equal pre-curvature and Poisson's ratio $\nu = 0.3$, are globally stable for maximum tip orientation angles, $\beta_1 = \beta_2$, that are less than 79°. There are many clinical applications, however, for which it is desirable for tip orientations to vary smoothly between $\pm 90°$ or even a wider range. Consequently, the development of techniques to increase the stability of concentric tube robots is important to expanding their clinical utility.

Based on (1), two possible approaches to enhancing stability are (i) to vary the tube properties so as to modify Poisson's ratio, or (ii) to consider pre-curvatures that vary with the arc length. This paper takes the latter approach and its contribution is to prove that, by employing tubes with pre-curvatures that vary with arc length, stability constraints on tube length, L, and tip orientation angle, β, can be eliminated. Furthermore, maximum curvature is bounded only by mechanical properties.

The remainder of the paper is organized as follows. The next section provides a concise statement of the mechanics-based model for the tubes. The subsequent section presents a

necessary and sufficient condition for evaluating the stability of a tube pair with non-constant pre-curvatures based on solving a linear ODE with specified boundary conditions. The approach is demonstrated analytically for two example pre-curvature functions. The subsequent section formulates the selection of pre-curvatures as an optimal design problem and provides both analytical and numerical examples. Conclusions are presented in the final section.

II. KINEMATICS OF PLANAR TUBE PAIR

The mechanics-based kinematic equations for a general concentric tube robot with n tubes are derived in [1] under the assumption of constant stiffness tensor $K_i \in \mathbb{R}^{3\times 3}$ and pre-curvature vector $\hat{u}_i = \begin{pmatrix} \hat{u}_{ix} & \hat{u}_{iy} & 0 \end{pmatrix}^T \in \mathbb{R}^3$. If the tubes have arc length-varying pre-curvature $\hat{u}_i(s) = \begin{pmatrix} \hat{u}_{ix}(s) & \hat{u}_{iy}(s) & \hat{u}_{iz}(s) \end{pmatrix}^T \in \mathbb{R}^3$, in which the z-component $\hat{u}_{iz}(s) \in \mathbb{R}$ is differentiable with respect to the arc length parameter s, similar derivations yield kinematic equations of the form

$$\begin{aligned}
\dot{\alpha}_i &= u_{iz} - u_{1z},\ i = 2, \ldots, n \\
u_{1z} &= \hat{u}_{1z} - \frac{1}{k_{1z}} \left(k_{2z}(u_{2z} - \hat{u}_{2z}) + \ldots + k_{nz}(u_{nz} - \hat{u}_{1z}) \right) \\
\dot{u}_{iz} &= \dot{\hat{u}}_{iz} + \frac{k_{ix}}{k_{iz}}(u_{ix}\hat{u}_{iy} - u_{iy}\hat{u}_{ix}) \\
u_i|_{x,y} &= \left(\left(\sum_{j=1}^{n} K_j \right)^{-1} R_z^T(\alpha_i) \left(\sum_{j=1}^{n} R_z(\alpha_j) K_j \hat{u}_j \right) \right) \Bigg|_{x,y}
\end{aligned} \tag{2}$$

where $\alpha_i \in \mathbb{R}$ is the relative twist angle between the first and i-th tubes and $u_i(s) = \begin{pmatrix} u_{ix}(s) & u_{iy}(s) & u_{iz}(s) \end{pmatrix}^T \in \mathbb{R}^3$ is the three-component curvature vector of the i-th tube. $R_z(\alpha)$ is rotation matrix for rotation of α about z-axis. K_i is assumed to be a diagonal matrix with diagonal components $k_{ix} \in \mathbb{R}$ and $k_{iz} \in \mathbb{R}$. These equations can be solved for the boundary conditions

$$u_{iz}(L_i) - \hat{u}_{iz}(L_i) = 0,\ i = 2, \ldots, n, \tag{3}$$

where L_i is the insertion length of the i-th tube. Usually, the base rotations α_{i0} are given as the kinematic inputs, which yields the following additional boundary conditions:

$$\alpha_i(0) = \alpha_{i0},\ i = 2, \ldots, n.$$

Consider a pair of tubes, $n = 2$, that have the same stiffness and planar pre-curvature in order for the combined shape of the tubes to straighten when the base rotation angle is π. The planar pre-curvature vector $\hat{u}_i$ and the stiffness tensor K_i can be defined as

$$\begin{aligned}
\hat{u}_i &= \begin{bmatrix} 0 \\ \hat{u}_y(s) \\ 0 \end{bmatrix},\ i = 1, 2 \\
K_i &= \begin{bmatrix} k_x & 0 & 0 \\ 0 & k_x & 0 \\ 0 & 0 & k_z \end{bmatrix},\ i = 1, 2.
\end{aligned}$$

For this tube pair, the kinematic equations (2) reduce to

$$\begin{aligned}
\dot{\alpha} &= u_{2z} - u_{1z} \\
u_{1z} &= -u_{2z} \\
u_{1x} &= -\frac{1}{2}\hat{u}_y(s)\sin\alpha \\
\dot{u}_{1z} &= \frac{k_x}{k_z} u_{1x} \hat{u}_y(s).
\end{aligned}$$

Combining the above equations yields a scalar second-order ordinary differential equation of the form

$$\ddot{\alpha} = \frac{k_x}{k_z}\hat{u}_y^2(s)\sin\alpha \tag{4}$$

with the boundary condition

$$\dot{\alpha}(L) = 0. \tag{5}$$

III. STABILITY CONDITION FOR PLANAR TUBE PAIRS

Since the differential equation (4) is second-order, there should be an additional boundary condition besides (5) in order to obtain a unique solution. Generally, a base rotation α_0 can be given as the boundary condition. In this case, however, it becomes a two-point boundary value problem for which multiple solutions can exist. On the other hand, if a rotation at the distal end of the robot α_L is given as the boundary condition, it becomes a backward initial value problem for which a unique solution exists. Let $\alpha(s, \alpha_L)$ denote the solution to (4) given the boundary conditions (5) and

$$\alpha(L) = \alpha_L. \tag{6}$$

Note that our study is focused on solutions for $\alpha_L \in [0, \pi]$ rather than $\alpha_L \in [0, 2\pi]$. The remaining $\alpha_L \in [\pi, 2\pi]$ provide symmetric solutions to those for $\alpha_L \in [0, \pi]$. As stated in [1], a stable tube pair features a curve in which α_0 increases monotonically with α_L, or equivalently,

$$\frac{\partial \alpha}{\partial \alpha_L}(0, \alpha_L) > 0 \text{ for } \alpha_L \in [0, \pi].$$

A result on the stability of tube pairs can be derived from the following proposition, whose proof can be found in the Appendix.

Proposition 1: Let $\alpha(s, \alpha_L)$ denotes the solution to (4)-(6). Then the condition

$$\frac{\partial \alpha}{\partial \alpha_L}(0, \alpha_L) > 0 \text{ for } \alpha_L \in [0, \pi]$$

is equivalent to

$$\frac{\partial \alpha}{\partial \alpha_L}(s, \pi) > 0 \text{ for } s \in [0, L]. \tag{7}$$

A physical interpretation of this proposition is possible by noting that $\alpha(s) = \pi$ is the solution to (4)-(6) when $\alpha_L = \pi$, for which the tube centerlines are straight. Imagine a small configuration change corresponding to a small negative variation of α_L at this configuration as depicted in Figure 2:

if the rotational displacement is always negative along the arc length, then from the proposition the tube pair is stable. The same explanation is possible with a positive variation and corresponding positive rotation along the arc length. We just choose the negative sign here in order to bound our scope within $\alpha_L \in [0, \pi]$. More precisely, consider the linear differential equation

$$\frac{d^2}{ds^2}\frac{\partial \alpha}{\partial \alpha_L}(s,\pi) = -\frac{k_x}{k_z}\hat{u}_y^2(s)\frac{\partial \alpha}{\partial \alpha_L}(s,\pi) \tag{8}$$

with boundary conditions

$$\frac{\partial \alpha}{\partial \alpha_L}(L,\pi) = 1, \quad \frac{d}{ds}\frac{\partial \alpha}{\partial \alpha_L}(L,\pi) = 0. \tag{9}$$

These equations are obtained by differentiating (4)-(6) with respect to α_L at $\alpha(s) = \pi$. If the solution to (8)-(9) is always positive over $s \in [0, L]$, the tube pair is stable. This allows us to determine the stability of the given tube pair by examining the solution of the linear differential equation for a set of specific boundary conditions, instead of solving (4) subject to the general boundary conditions (5) and (6) for $\alpha_L \in [0, \pi]$.

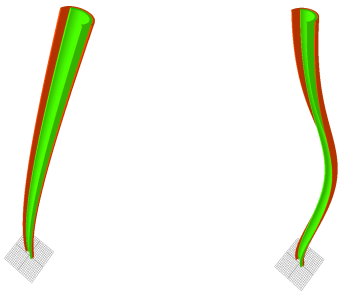

Fig. 2. Configurations of stable (left) and unstable (right) tubes slightly varied from straight configurations. Tubes are assumed to have constant pre-curvature. Stable tubes generate consistent direction of relative rotation along arc length while unstable tubes does not. Half of each tube is not visualized to see the inner rotation.

IV. EVALUATING STABILITY FOR SPECIFIC PRE-CURVATURE FUNCTIONS

To both validate and demonstrate the applicability of our stability results, we now consider two examples in which the pre-curvature is prescribed analytically. In the first example, we show that for the constant pre-curvature case, our stability result reduces to the previously published result given by (1). The second example considers pre-curvatures of the form $\hat{u}_y = \frac{b}{s+a}$ with $\{a, b\} \in \mathbb{R}^+$.

A. Constant Pre-curvature

If $\hat{u}_y$ is a constant function, there exists an analytic solution to (8) given by

$$\frac{\partial \alpha}{\partial \alpha_L}(s,\pi) = \cos\left(\sqrt{\frac{k_x}{k_z}}\hat{u}_y(L-s)\right).$$

To satisfy (7), the inequality

$$\sqrt{\frac{k_x}{k_z}}\hat{u}_y(L-s) < \frac{\pi}{2}$$

must hold for any $s \in [0, L]$. Since the left side attains the maximum value at $s = 0$, the inequality reduces to

$$\sqrt{\frac{k_x}{k_z}}\hat{u}_y L < \frac{\pi}{2}, \tag{10}$$

which is the same result reported in [1].

B. Pre-curvature Function, $\hat{u}_y = \frac{b}{s+a}$

Assume that $\hat{u}_y(s) = \frac{b}{s+a}$ with positive scalars $a \in \mathbb{R}^+$ and $b \in \mathbb{R}^+$. The analytic solution to (8) is given by

$$\frac{\partial \alpha}{\partial \alpha_L}(s,\pi) = \begin{cases} -\frac{c_2}{c_1}\left(\frac{s+a}{L+a}\right)^{c_3} + \frac{c_3}{c_1}\left(\frac{s+a}{L+a}\right)^{c_2} & \text{if } c_0 < \frac{1}{4} \\ \sqrt{\frac{s+a}{L+a}}\left(1 - \frac{1}{2}\ln\frac{s+a}{L+a}\right) & \text{if } c_0 = \frac{1}{4} \\ -\frac{c_0}{c_5}\sqrt{\frac{s+a}{L+a}}\sin\left(c_5 \ln\frac{s+a}{L+a} - c_6\right) & \text{if } c_0 > \frac{1}{4} \end{cases} \tag{11}$$

where

$$c_0 = \frac{k_x}{k_z}b^2, \;\; c_1 = \sqrt{1-4c_0}, \;\; c_2 = \frac{1}{2} - \sqrt{\frac{1}{4} - c_0}$$
$$c_3 = \frac{1}{2} + \sqrt{\frac{1}{4} - c_0}, \;\; c_4 = \sqrt{\frac{1}{4} + c_0}, \;\; c_5 = \sqrt{c_0 - \frac{1}{4}}$$
$$c_6 = \tan^{-1} 2c_3.$$

When $c_0 \leq \frac{1}{4}$, it is easily shown that $\frac{\partial \alpha}{\partial \alpha_L}(s,\pi) > 0$ for $s \in [0, L]$; In other words, it can be verified that the tube pair is stable simply by checking $\frac{\partial \alpha}{\partial \alpha_L}(0,\pi) > 0$ and $\frac{d}{ds}\frac{\partial \alpha}{\partial \alpha_L}(s,\pi) \geq 0$. This implies that any pre-curvature with (a, b) satisfying $c_0 \leq \frac{1}{4}$ can be used for a stable tube pair. Since c_0 is invariant to a, the choice of a is unbounded in $\mathbb{R}^+$. Defining the central angle θ_{tip} swept out by the initial curvature of the tubes as

$$\theta_{tip} = \int_0^L \hat{u}_y ds = b \ln\frac{L+a}{a},$$

an arbitrarily large θ_{tip} can be achieved by selecting a to be a very small positive scalar. From a theoretical perspective, this result is quite meaningful, since the swept angle θ_{tip} is bounded by the inequality (10) for the constant pre-curvature case. A more detailed discussion is presented in Section V.

On the other hand, when $c_0 > \frac{1}{4}$, the following inequality must hold in order to satisfy $\frac{\partial \alpha}{\partial \alpha_L}(s) > 0$:

$$\sqrt{c_0 - \frac{1}{4}}\ln\frac{s+a}{L+a} - \tan^{-1} 2\sqrt{c_0 - \frac{1}{4}} > -\pi.$$

Noting that the left side attains a minimum at $s = 0$, the inequality reduces to

$$\frac{a}{L} > \left(\exp\frac{\pi - \tan^{-1} 2\sqrt{c_0 - \frac{1}{4}}}{\sqrt{c_0 - \frac{1}{4}}} - 1\right)^{-1}. \tag{12}$$

In practice it is hard to achieve $c_0 \leq \frac{1}{4}$ due to the yield strain of the material used for tubes, which is also discussed in more detail in Section V. The inequality (12) should in practice be regarded as a general stability condition for the pre-curvature $\hat{u}_y = \frac{b}{s+a}$.

The stability condition (12) can be validated by plotting α_0 versus α_L curves for various (a, b) pairs. The curves are depicted in Figure 3. To plot each curve in the figure, α_L is discretized into 21 values between 0 and 2π and given as

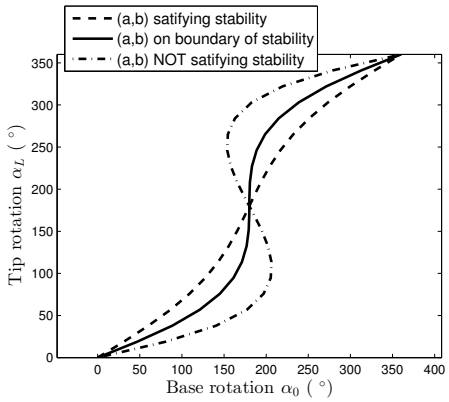

Fig. 3. α_0 versus α_L curves for various (a, b) pairs.

boundary conditions for the general kinematic equations (2). If a pair (a, b) satisfies the stability condition (12), the curve is monotonically increasing as expected. Similarly, for a pair (a, b) on the boundary of the inequality (12), the curve is still increasing, but possesses an infinitely steep slope at $(\alpha_0, \alpha_L) = (\pi, \pi)$. Otherwise, the slope is negative over some parts of the curve.

V. FORMULATION AS AN OPTIMAL DESIGN PROBLEM

It is possible to formulate the selection of pre-curvatures as an optimal design problem. Given a desired value of θ_{tip}, a tube pair is stable if and only if the solution to (4)-(6), $\alpha(s, \alpha_L)$, satisfies the inequality

$$\frac{\partial \alpha}{\partial \alpha_L}(0, \alpha_L) > 0 \text{ for } \alpha_L \in [0, \pi]. \tag{13}$$

If there exist multiple pre-curvature function candidates that satisfy (13), it is desirable to choose the most stable solution. Note that $\frac{\partial \alpha}{\partial \alpha_L}(0, \alpha_L)$ is the inverse slope of α_0 versus α_L curve. If this value is excessively small (but still positive) for some value of $\alpha_L \in [0, \pi]$, even a small base rotation can cause the tube pair to snap very quickly. An optimal pre-curvature can therefore be defined as one that maximizes the minimum value of $\frac{\partial \alpha}{\partial \alpha_L}(0, \alpha_L)$ over $\alpha_L \in [0, \pi]$. The resulting optimal design problem is formulated as follows.

$$\max_{\hat{u}_y(s)} \left(\min_{\alpha_L} \frac{\partial \alpha}{\partial \alpha_L}(0, \alpha_L) \right)$$

subject to the constraints

$$\begin{aligned} \int_0^L \hat{u}_y(s) ds &= \theta_{tip} \\ \frac{\partial \alpha}{\partial \alpha_L}(0, \alpha_L) &> 0. \end{aligned}$$

If $\frac{\partial \alpha}{\partial \alpha_L}(0, \alpha_L) > 0$, then it satisfies

$$\min_{\alpha_L} \frac{\partial \alpha}{\partial \alpha_L}(s, \alpha_L) = \frac{\partial \alpha}{\partial \alpha_L}(s, \pi) \tag{14}$$

for any $s \in [0, L]$; this is proven in Proposition 3, which is used in the proof of Proposition 1 given in the appendix.

Using (14) and Proposition 1 to respectively reformulate the cost function and the last constraint, the optimization reduces equivalently to

$$\max_{\hat{u}_y(s)} \frac{\partial \alpha}{\partial \alpha_L}(0, \pi) \tag{15}$$

subject to the modified constraints

$$\begin{aligned} \int_0^L \hat{u}_y(s) ds &= \theta_{tip} \\ \frac{\partial \alpha}{\partial \alpha_L}(s, \pi) &> 0. \end{aligned}$$

In practice, a high pre-curvature causes yielding problems, especially when the tubes are straightened. One possible pre-curvature function that does not cause yielding is given by

$$\hat{u}_y(s) < \frac{2\bar{\epsilon}}{d(\bar{\epsilon} + 1)}$$

where $\bar{\epsilon}$ and d are the yield strain and outer diameter of the tube, respectively. To include this feature in the optimization, one can add the constraint

$$\hat{u}_y(s) \leq \hat{u}_{max} \tag{16}$$

to the optimization, with $\hat{u}_{max}$ chosen to satisfy $\hat{u}_{max} < \frac{2\bar{\epsilon}}{d(\bar{\epsilon}+1)}$.

A. Analytical Solution to the Optimal Design Problem

In some cases, it is possible to solve the design problem analytically when a pre-curvature function is specified. As an example, consider again the pre-curvature function $\hat{u}_y = \frac{b}{s+a}$ with positive scalars $a \in \mathbb{R}^+$ and $b \in \mathbb{R}^+$. Then the optimization (15) and constraint (16) reduce to

$$\max_{a,b>0} \frac{\partial \alpha}{\partial \alpha_L}(0, \pi) \tag{17}$$

subject to

$$b \ln \frac{L + a}{a} = \theta_{tip}, \tag{18}$$

$$\frac{\partial \alpha}{\partial \alpha_L}(s, \pi) > 0, \tag{19}$$

$$\frac{b}{a} \leq \hat{u}_{max}. \tag{20}$$

Substituting (18) and $s = 0$ into (11) yields

$$\frac{\partial \alpha}{\partial \alpha_L}(0, \pi) = f(b)$$

which is a function of b only. By differentiating $f(b)$ with respect to b, it is possible to show that $\frac{df}{db}(b) < 0$ under the stability condition given in Section IV-B. Maximizing $f(b)$ is thus equivalent to minimizing b subject to the constraint (20). Combining (18) with (20) leads to

$$b \left(\exp \frac{\theta_{tip}}{b} - 1 \right) \leq \hat{u}_{max} L. \tag{21}$$

Let $g(b)$ denote the left side of the inequality. Then the first and second derivatives with respect to b are given by

$$\begin{aligned} g'(b) &= \left(1 - \tfrac{\theta_{tip}}{b}\right) \exp \tfrac{\theta_{tip}}{b} - 1 \\ g''(b) &= \tfrac{\theta_{tip}}{b} \exp \tfrac{\theta_{tip}}{b}. \end{aligned}$$

Since $g''(b) > 0$ and $\lim_{b\to\infty} g'(b) = 0$ for any positive scalar b, $g(b)$ is a decreasing function of $b \in \mathbb{R}^+$. Consequently, the minimum value of b is the root of (21) when the equality holds. a is then given by

$$a = \frac{L}{\exp\frac{\theta_{tip}}{b} - 1}.$$

Note that there does not exist multiple roots for b because $g(b)$ is monotonically decreasing.

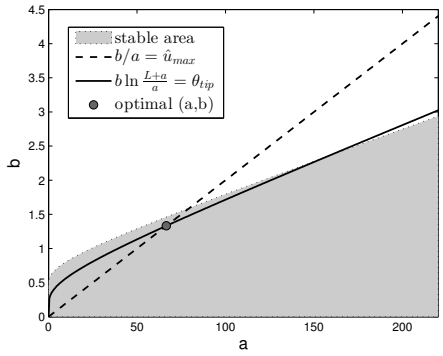

Fig. 4. Optimal (a, b) plotted on the a-b plane with the corresponding stability condition and constraints.

Geometrically, the optimizer is located at the intersection point of (18) and (20). An example is depicted in Figure 4 in the case when $\theta_{tip} = 90°$, $\hat{u}_{max} = \frac{1}{50mm}$, and $L = 150mm$. The shaded region is the stable area for which the pair (a, b) satisfies the stability condition described in Section IV-B. If the constraints are tightened by reducing $\hat{u}_{max}$ or increasing θ_{tip}, the problem may no longer be feasible, as the intersection point lies outside the shaded stable region.

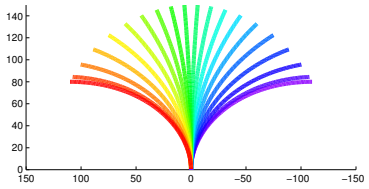

Fig. 5. Combined curvature of the analytic solution with varying base rotation.

The combined curvature and α_0 versus α_L curve of the analytic solution are given in Figures 5 and 6, respectively. As shown in the α_0 versus α_L curve, the tube pair is stable for the central angle $\theta_{tip} = 90°$, which cannot be achieved by a constant pre-curvature.

B. Numerical Solution of the Optimal Design Problem

As an alternative to specifying a pre-curvature function a priori, numerical techniques can be used to generate solutions. A simple way to solve the problem defined above is to recast it in the form of an optimal control problem

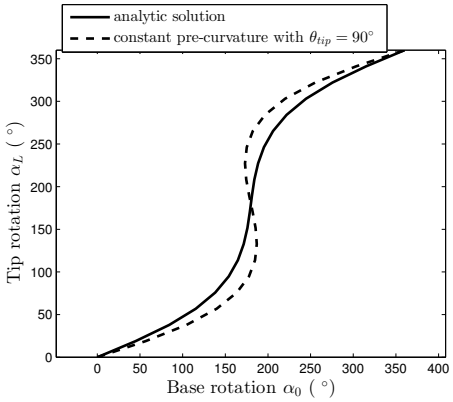

Fig. 6. α_0 versus α_L curve of analytic solution compared with constant pre-curvature.

and to employ, e.g., the steepest descent method described in [10].

For notational simplicity, we define

$$x_1(s) = \frac{\partial\alpha}{\partial\alpha_L}(s,\pi), \quad x_2(s) = \frac{d}{ds}\frac{\partial\alpha}{\partial\alpha_L}(s,\pi).$$

Equation (8) and the boundary conditions (9) can then be written

$$\begin{pmatrix} \dot{x}_1(s) \\ \dot{x}_2(s) \end{pmatrix} = \begin{pmatrix} x_2(s) \\ -\frac{k_x}{k_z}\hat{u}_y^2(s)x_1(s) \end{pmatrix}, \; x(L) = \begin{pmatrix} 1 \\ 0 \end{pmatrix}. \tag{22}$$

The cost function to be minimized is given by

$$J = -\frac{\partial\alpha}{\partial\alpha_L}(0,\pi) = \int_0^L x_2(s)ds - 1.$$

Ignoring the constant term -1, the Hamiltonian and costate equation are respectively given by

$$\mathcal{H} = x_2(s) + p_1(s)x_2(s) - \frac{k_x}{k_z}\hat{u}_y^2(s)p_2(s)x_1(s)$$

$$\begin{pmatrix} \dot{p}_1(s) \\ \dot{p}_2(s) \end{pmatrix} = \begin{pmatrix} \frac{k_x}{k_z}\hat{u}_y^2(s)p_2(s) \\ -1 - p_1(s) \end{pmatrix}, \; p(0) = \begin{pmatrix} 0 \\ 0 \end{pmatrix}. \tag{23}$$

The update direction $\frac{dH}{du}$ is given by

$$\frac{d\mathcal{H}}{du} = -2\frac{k_x}{k_z}\hat{u}_y(s)p_2(s)x_1(s). \tag{24}$$

In the numerical implementation, the constraints $\hat{u}_y(s) \le u_{max}$ and $\int_0^L \hat{u}_y(s)ds = \theta_{tip}$ are given as linear constraints of the form

$$\hat{u}_y^i \le u_{max}, \; i = 1, \ldots, N$$

$$\sum_{i=1}^{N} \hat{u}_y^i \Delta s = \theta_{tip}$$

where N is the dimension of $\hat{u}_y$ discretized by the step size Δs, and $\hat{u}_y^i$ is its i-th component. Then $\frac{dH}{du}$ is the N-dimensional gradient vector of the cost J, which can be computed by solving the initial value problem (22), (23) and Equation (24) sequentially. Since the steepest descent method

does not guarantee a global minimizer, the analytic solution in Section V-A is used as the initial guess. The results and comparison with the analytic solution are given in Figures 7 and 9.

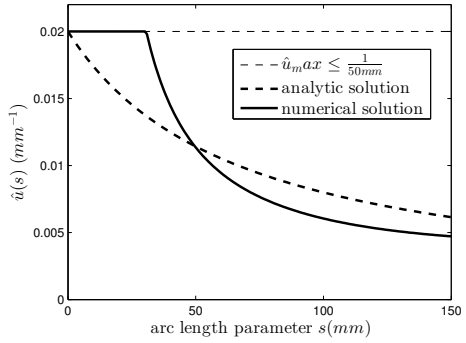

Fig. 7. Analytic and numerical solutions.

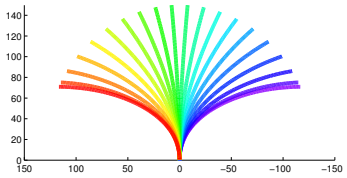

Fig. 8. Combined curvature of numerical solution with varying base rotation.

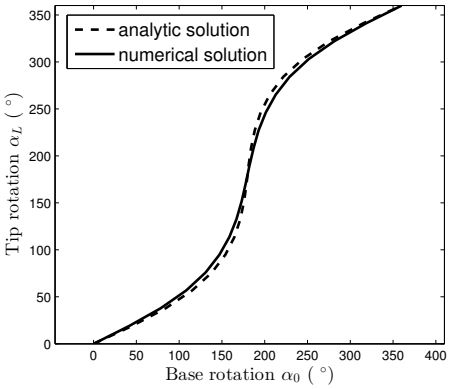

Fig. 9. α_0 versus α_L curves of analytic and numerical solutions.

In Figure 7, the numerical solution tends to a have higher pre-curvature at the base and lower pre-curvature at the distal end. If the pre-curvature is high at the distal end, both tubes are bound to each other tightly at the distal end, causing a large twist along the arc length as the base rotates. Consequently, this increases the possibility of a rapid untwisting motion by a sudden release of the stored energy. By reducing the pre-curvature at the distal end, the numerical solution shows more stable behaviour, as its α_0 versus α_L curve is straighter than that of the analytic solution as depicted in Figure 9.

VI. CONCLUSIONS

Prior concentric tube robot designs have considered tubes of piecewise-constant pre-curvature for reasons of simplicity and also since the combined tube shape is approximately piecewise constant. The results of this paper demonstrate, however, that stability is enhanced for curvatures that decrease with increasing arc length. In comparison with prior stability results for constant tube pre-curvatures, this approach removes the limits on both tip orientation range and tube length. The price paid for enhanced stability, though, is a larger average robot radius of curvature.

In the approach proposed in [1], concentric tube robots are designed as telescoping concatenations of variable and fixed curvature sections. Variable curvature sections correspond directly to the planar tube pairs considered in this paper. Consequently, the new stability results can be directly incorporated into this design framework to create designs with larger stable workspaces.

APPENDIX
PROOF OF PROPOSITION 1

We first prove the following two propositions:

Proposition 2: Let $\alpha(s, \alpha_L)$ denotes the solution to (4)-(6). Then

$$\frac{\partial \alpha}{\partial \alpha_L}(0, \alpha_L) > 0 \text{ for } \alpha_L \in [0, \pi] \tag{25}$$

if and only if

$$\frac{\partial \alpha}{\partial \alpha_L}(s, \alpha_L) > 0 \text{ for } s \in [0, L] \text{ and } \alpha_L \in [0, \pi].$$

Proof: The backward direction is obvious, requiring only proof of the forward direction. For notational simplicity, $\frac{\partial \alpha}{\partial \alpha_L}$ is replaced by $x = \frac{\partial \alpha}{\partial \alpha_L}$. Differentiating (4)-(6) with respect to α_L yields a linear ODE

$$\ddot{x}(s, \alpha_L) = \frac{k_x}{k_z} \hat{u}_y^2(s) \cos(\alpha) x(s, \alpha_L) \tag{26}$$

with boundary conditions

$$x(L, \alpha_L) = 1, \quad \dot{x}(L, \alpha_L) = 0. \tag{27}$$

When $\alpha_L = 0$, the solution to (4)-(6) is $\alpha(s, 0) = 0$. In this case, Equation (26) reduces to

$$\ddot{x}(s, 0) = \frac{k_x}{k_z} \hat{u}_y^2(s) x(s, 0).$$

Given the boundary conditions (27) together with a positive value of $\frac{k_x}{k_z} \hat{u}_y^2(s)$, $x(s, 0)$ results in a decreasing function in $s \in [0, L]$, which satisfies $x(s, 0) \geq 1$.

Suppose there exists a solution to (26), $x(s, \gamma)$, which is not always positive in $s \in [0, L]$. Differentiating Equation (26) again with respect to α_L yields

$$\begin{aligned} \frac{d^2}{ds^2} \frac{\partial x}{\partial \alpha_L}(s, \alpha_L) \quad &= \tfrac{k_x}{k_z} \hat{u}_y^2(s) \cos(\alpha) \tfrac{\partial x}{\partial \alpha_L}(s, \alpha_L) \\ &\quad - \tfrac{k_x}{k_z} \hat{u}_y^2(s) \sin(\alpha) x^2(s, \alpha_L) \end{aligned}$$

Since this is also a linear ODE in $\frac{\partial x}{\partial \alpha_L}(s, \alpha_L)$ for which the system input is associated with $x(s, \alpha_L)$, it leads to a finite value of $\frac{\partial x}{\partial \alpha_L}(s, \alpha_L)$ for a finite $x(s, \alpha_L)$. Consequently, $x(s, \alpha_L)$ as well as its minimum value over $s \in [0, L]$ is continuously varying over $\alpha_L \in [0, \gamma]$. Since the minimum value of $x(s, \gamma)$ is not positive while that of $x(s, 0)$ is 1, there exists at least one α_L between 0 and γ for which the minimum value of $x(s, \alpha_L)$ is zero. Let β and t denote this α_L and corresponding minimizer, respectively. Then

$$x(t, \beta) = 0. \tag{28}$$

By (25) and (27), t is neither 0 nor L. The first-order necessary condition for the minimizer t which is not on the boundary of the domain $s \in [0, L]$ is given by

$$\dot{x}(t, \beta) = 0. \tag{29}$$

However, this is not possible since the only solution to (26) given (28) and (29) is a constant function $x(s, \beta) = 0$, which does not satisfy the boundary condition (27). Thus, there does not exist any solution to (26) that is not always positive in $s \in [0, L]$.

■

Proposition 3: Let $\alpha(s, \alpha_L)$ denote the solution to (4)-(6). If

$$\frac{\partial \alpha}{\partial \alpha_L}(s, \pi) > 0 \text{ for } s \in [0, L], \tag{30}$$

then it satisfies

$$\frac{\partial \alpha}{\partial \alpha_L}(s, \alpha_L) \geq \frac{\partial \alpha}{\partial \alpha_L}(s, \pi)$$

for any $s \in [0, L]$ and $\alpha_L \in [0, \pi]$.

Proof: Let x denote $\frac{\partial \alpha}{\partial \alpha_L}$ again. By differentiating (4)-(6) with respect to α_L, the same equations (26)-(27) are obtained. When $\alpha_L = \pi$, the solution to (4)-(6) is $\alpha(s, \pi) = \pi$. In this case, Equation (26) reduces to

$$\ddot{x}(s, \pi) = -\frac{k_x}{k_z} \hat{u}_y^2(s) x(s, \pi).$$

The proposition is clearly satisfied when $s = L$ or $\alpha_L = \pi$. Suppose there exists $t \in [0, L)$ and $\beta \in [0, \pi)$ that does not satisfy the proposition, i.e.,

$$x(t, \beta) < x(t, \pi). \tag{31}$$

By (30), the following inequalities hold:

$$\ddot{x}(s, \pi) \leq \frac{k_x}{k_z} \hat{u}_y^2(s) \cos\left(\alpha(s, \beta)\right) x(s, \pi),$$
$$x(t, \pi) \geq x(t, \beta), \quad x(L, \pi) \geq x(L, \beta)$$

These are the conditions for $x(s, \pi)$ to be an upper solution [11] to $x(s, \beta)$ over $s \in [t, L]$. It has been proven that any solution to an ODE lies below the upper solution. However, because of the same boundary conditions $x(L, \beta) = x(L, \pi) = 1$, $\dot{x}(L, \beta) = \dot{x}(L, \pi) = 0$ and the smaller value of the second derivative

$$\left\{ \ddot{x}(L, \pi) = -\frac{k_x}{k_z} \hat{u}_y^2(L) \right\} < \left\{ \ddot{x}(L, \beta) = \frac{k_x}{k_z} \hat{u}_y^2(L) \cos(\beta) \right\},$$

it follows that $x(t, \pi)$ cannot be the upper solution near $s = L$. This can be shown via a Taylor expansion for a small positive scalar ϵ:

$$x(L - \epsilon, \pi) - x(L - \epsilon, \beta) \approx \frac{1}{2} \epsilon^2 \left(\ddot{x}(L, \pi) - \ddot{x}(L, \beta) \right) < 0$$

Thus, there does not exist any $t \in [0, L)$ and $\beta \in [0, \pi)$ satisfying (31).

■

The forward direction of Proposition 1 is satisfied straightforwardly by Proposition 2. The backward direction is also satisfied by Proposition 3, i.e.,

$$\frac{\partial \alpha}{\partial \alpha_L}(s, \alpha_L) \geq \frac{\partial \alpha}{\partial \alpha_L}(s, \pi) > 0.$$

ACKNOWLEDGMENT

Junhyoung Ha and Frank C. Park were supported by grants from the Biomimetic Robotics Research Center, SNU-IAMD, and the SNU BK21+ Program in Mechanical Engineering.

REFERENCES

[1] P. E. Dupont, J. Lock, B. Itkowitz, and E. Butler, "Design and control of concentric-tube robots," *IEEE Trans. Robotics*, vol. 26, no. 2, pp. 209–225, 2010.

[2] D. C. Rucker, R. J. Webster, G. S. Chirikjian, and N. J. Cowan, "Equilibrium conformations of concentric-tube continuum robots," *The International Journal of Robotics Research*, vol. 29, no. 10, pp. 1263–1280, 2010.

[3] R. Xu and R. Patel, "A fast torsionally compliant kinematic model of concentric-tube robots," in *Engineering in Medicine and Biology Society (EMBC), 2012 Annual International Conference of the IEEE*, pp. 904–907, IEEE, 2012.

[4] T. Anor, J. R. Madsen, and P. Dupont, "Algorithms for design of continuum robots using the concentric tubes approach: a neurosurgical example," in *Robotics and Automation (ICRA), 2011 IEEE International Conference on*, pp. 667–673, IEEE, 2011.

[5] J. Burgner, P. Swaney, R. Lathrop, K. Weaver, and R. Webster, "Debulking from within: A robotic steerable cannula for intracerebral hemorrhage evacuation.," *IEEE transactions on bio-medical engineering*, 2013.

[6] A. H. Gosline, N. V. Vasilyev, E. J. Butler, C. Folk, A. Cohen, R. Chen, N. Lang, P. J. Del Nido, and P. E. Dupont, "Percutaneous intracardiac beating-heart surgery using metal MEMS tissue approximation tools," *The International journal of robotics research*, vol. 31, no. 9, pp. 1081–1093, 2012.

[7] N. V. Vasilyev, A. H. Gosline, E. Butler, N. Lang, P. J. Codd, H. Yamauchi, E. N. Feins, C. R. Folk, A. L. Cohen, R. Chen, *et al.*, "Percutaneous steerable robotic tool delivery platform and metal MEMS device for tissue manipulation and approximation closure of patent foramen ovale in an animal model," *Circulation: Cardiovascular Interventions*, vol. 6, no. 4, pp. 468–475, 2013.

[8] C. Bergeles and P. E. Dupont, "Planning stable paths for concentric tube robots," in *Intelligent Robots and Systems (IROS), 2013 IEEE/RSJ International Conference on*, pp. 3077–3082, IEEE, 2013.

[9] P. E. Dupont, J. Lock, and E. Butler, "Torsional kinematic model for concentric tube robots," in *Robotics and Automation, 2009. ICRA'09. IEEE International Conference on*, pp. 3851–3858, IEEE, 2009.

[10] D. Kirk, "Optimal control theory: an introduction," *Prentice-Hall network series*, 1970.

[11] C. Alberto, "An overview of the lower and upper solutions method with nonlinear boundary value conditions," *Boundary Value Problems*, vol. 2011, 2010.